Abstract

This work presents a physics-infused reduced-order modeling (PIROM) framework towards the design, analysis, and optimization of ablating hypersonic thermal protection systems (TPS).

1 Introduction

At hypersonic speeds, aerospace vehicles experience extreme aero-thermal environments that requires specialized thermal protection systems (TPS) to shield internal sub-structures, electronics, and possibly crew members from the intense aerodynamic heating. The TPS is often composed of ablating materials – a high-temperature capable fibrous material injected with a resin that fills the pore network and strengthens the composite Amar2016. The TPS design promotes the exchange of mass through thermal and chemical reactions (i.e., pyrolisis), effectively mitigating heat transfer to the sub-structures.

As a result, accurate prediction for the ablating TPS response under extreme hypersonic heating becomes fundamental to ensuring survivability, performance, and safety of hypersonic vehicles. Not only is it necessary to assess the performance of the thermal management systems, but also the shape changes of the vehicle's outer surface induced by the ablating material, and its impact on the aerodynamics, structural integrity, and controllability. Unfortunately, high-fidelity simulations of ablating TPS remains a formidable challenge both theoretically and computationally.

On the theoretical side, the thermo-chemical reactions, coupled with the irregular pore network structure, translate into simplifying assumptions to reduce non-linearities, and make the resulting equations more amenable for engineering application and design analysis x. For instance, one of the most notable codes is the one-dimensional CMA code that was developed by Aerotherm Corporation in the 1960s Howard2015. Despite its practical use in...

Another example is the CHarring Ablator Response (CHAR) ablation code, which ignores elemental decompositions of the pyrolizing gases, assumes the gases to be a mixture of perfect gases in thermal equilibrium, and assumes no reaction or condensation with the porous network [**?**].

theoretically:

computationally:

2 Modeling of Ablating Thermal Protection Systems

This section presents the ablation problem for a non-decomposing TPS as a parametrized system of non-linear PDEs. These non-linear PDEs govern the energy of heat conduction and the pseudo-elastic material deformation of the mesh motion. Two different but mathematically-connected numerical solution strategies are provided: (1) a high-fidelity full-order model (FOM) based on a discontinuous Galerkin FEM, and (2) a thermo-elastic RPM based on a one-dimensional approximation to the energy and pseudo-elasticity equations.

2.1 Governing Equations

Consider a generic domain $\Omega \subset$, $d = 2$ or 3, illustrated in Fig. 1. A heat flux $q_b(x,t)$ is prescribed on the boundary Γ_q (i.e., Neumann boundary condition), and the temperature $T_b(x,t)$ is prescribed on boundary Γ_T (i.e., Dirichlet boundary condition), where $\Gamma_q \cup \Gamma_T = \partial\Omega$ and $\Gamma_q \cap \Gamma_T = \emptyset$. The ablation occurs only on the heated boundary Γ_q, and its effects are included into the energy equation using an Arbitrary Lagrangian-Eulerian (ALE) description. The ALE assumes that the displacement $\mathbf{w}(x,t) \in \mathbb{R}^d$ of the computational mesh moves with velocity $\mathbf{v}(x,t)$ that is different to the material velocity, which is fixed to zero in this work.

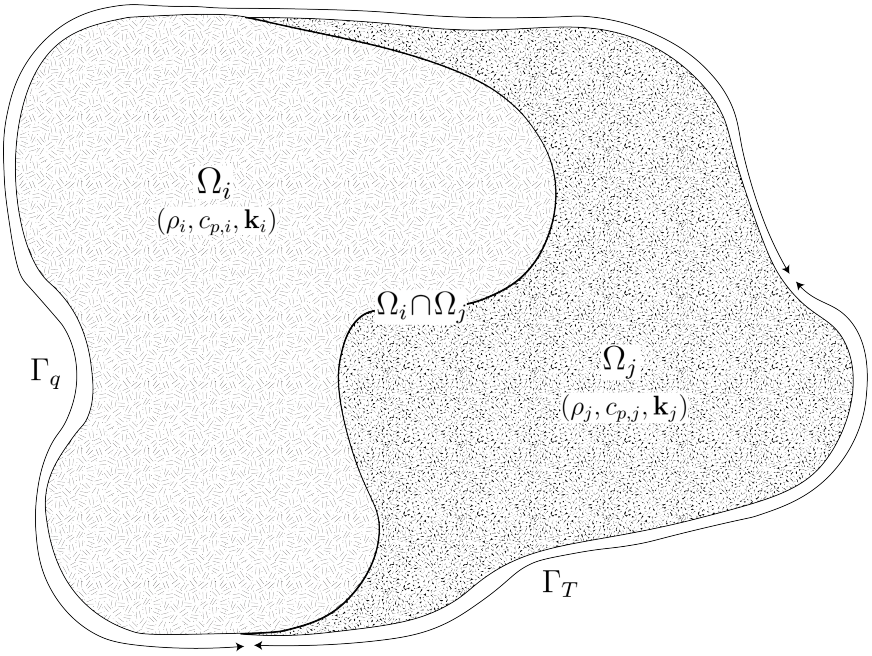

Figure 1: General domain Ω with prescribed heat flux $q_b(x,t)$ and temperature $T_b(x,t)$ on the boundaries Γ_q and Γ_T, respectively. The mesh moves with a velocity $\mathbf{v}(x,t)$, while the material velocity is $\mathbf{w}(x,t)$. draw mesh next to arbitrary domain with moving boundaries.

The transient heat conduction over the moving mesh is described by the following equations,

$$\rho c_p \left(\frac{\partial T}{\partial t} - \mathbf{v}(x,t) \cdot \nabla T \right) - \nabla \cdot (\mathbf{k} \nabla T) = \mathcal{Q}(x,t), \ x \in \Omega \tag{1a}$$

$$\nabla \cdot \boldsymbol{\sigma}(\mathbf{w}) = 0 \tag{1b}$$

$$-\mathbf{k}\nabla T \cdot \mathbf{n} = q_b(x,t), \ x \in \Gamma_q \tag{1c}$$

$$T(x,t) = T_b(x,t), \ x \in \Gamma_T \tag{1d}$$

$$T(x,0) = T_0(x), \ x \in \Omega \tag{1e}$$

$$\mathbf{w}(x,t) = \mathbf{w}_q(x,t), \quad x \in \Gamma_q \tag{1f}$$

$$\mathbf{w}(x,t) = 0, \quad x \notin \Gamma_q \tag{1g}$$

$$\mathbf{w}(x,t) = \mathbf{0} \tag{1h}$$

The density ρ, heat capacity c_p, and thermal conductivity $\mathbf{k} \in \mathbb{R}^{n_d \times n_d}$ are assumed to be constant with respect to temperature in this work. The terms in eq. (1a), in the order they appear, correspond to the unsteady energy storage, heat conduction, temperature advection due to mesh motion, and the heat source terms.

The elasticity equation eq. (1b) states that the divergence of the stress tensor $\boldsymbol{\sigma}(\mathbf{w})$ is zero. The stress tensor is related to the strain tensor $\boldsymbol{\epsilon}(\mathbf{w})$ through Hooke's law,

$$\boldsymbol{\sigma}(\mathbf{w}) = \mathbb{D} : \boldsymbol{\epsilon}(\mathbf{w})$$

where $\mathbb{D}$ is the constitutive operator, ":" is the double contraction of tensors, and $\boldsymbol{\epsilon}$ is the symmetric strain tensor given by,

$$\boldsymbol{\epsilon}(\mathbf{w}) = \frac{1}{2} \left(\nabla \mathbf{w} + \nabla \mathbf{w}^T \right)$$

For instance, an isotropic material assumption results in,

$$\boldsymbol{\sigma} = \lambda \left(\nabla \cdot \mathbf{w} \right) \mathbf{I} + 2\mu \boldsymbol{\epsilon}(\mathbf{w})$$

where λ and μ are Lame constants that are arbitrarily selected to model the mesh motion. The "material" properties λ and μ can be chosen to tailor the mesh deformation and need not represent the actual material being modeled Amar2016.

The boundary conditions for the energy equation includes a heated surface (eq. (1c)) and a constant-temperature surface (eq. (1d)). The boundary conditions for the pseudo-elasticity equation are a function of the surface temperature $T_q(x,t)$ for $x \in \Gamma_q$ using a B' table. The B' table....

$$\mathbf{w}_q(x,t) = \int_0^t \mathbf{v}(x,\tau)d\tau = \int_0^t \mathbf{f}\left(T_q(x,\tau)\right) d\tau \tag{2}$$

2.2 Full-Order Model: Discontinuous Galerkin Finite Element Method

To obtain the full-order numerical solution, the governing equation is spatially discretized using variational principle of Discontinuous Galerkin (DG) to result in a high-dimensional system of ODEs for the time-varying nodal data. The full-order TPS ablation simulations are computed using standard FEM instead, and the equivalence between DG and standard FEM is noted upon their convergence.

Consider a conforming mesh partition domain, where each element belongs to one and only one component. Denote the collection of all M elements as $\{E_i\}_{i=1}^M$. In an element E_i, its shared boundaries with another element E_j, Neumann BC, and Dirichlet BC are denoted as e_{ij}, e_{iq}, and e_{iT}, respectively. Lastly, $|e|$ denotes the length ($n_d = 2$) or area ($n_d = 3$) of a component boundary e.

For the e-th element, use a set of $n^{(e)}$ trial functions, such as polynomials, to represent the temperature distribution,

$$T^{(e)}(x,t) = \sum_{i=1}^{n^{(e)}} \phi_i^{(e)}(x) u_i^{(e)} \equiv \boldsymbol{\phi}^{(e)}(x)^T \mathbf{u}^{(e)}(t) \tag{3}$$

2.2.1 Numerical Solution

2.2.2 Usage Within an Ablation Simulation

2.3 Reduced-Physics Model: One-Dimensional Thermo-Elastic Solver

In this section, the main results regarding the derivation of the thermo-elastic RPM are presented, with the details provided in Appendix x. The thermo-elastic RPM is derived to model the one-dimensional temperature distribution and surface recession for an ablating TPS. The temperature is modeled using a coarse-grained DG-FEM approach, while the moving mesh is modeled using an analytical solution to the elasticity equations.

Consider the partitioning of the general domain depicted in Fig. 1 into $N = 3$ non-overlapping interconnected components $\{\Omega_i\}_{i=1}^3$, as illustrated in Fig. 2. The coupling between the components is due to the volumetric energy source terms,

$$\mathcal{Q}_{\text{net}}^{(1)}(x,t), \quad \mathcal{Q}_{\text{net}}^{(2)}(x,t), \quad \mathcal{Q}_{\text{net}}^{(3)}(x,t)$$

which are space-time varying, and are unknown quantities due to the moving interfaces between the interconnected components.

where the thermodynamic coupling occurs due to $\mathcal{Q}^{(1,2)}(x,t)$ and $\mathcal{Q}^{(2,3)}(x,t)$, which are space-time varying. The i-th component Ω_i is associated with material properties $\left\{\rho^{(i)}, c_p^{(i)}, k^{(i)}\right\}$, which are continuous within each component, and may be discontinuous across two neighboring components.

A first-order DG-FEM scheme is adopted for each component, with the coupling between the components enforced via interior point penalty methods x as discussed in Sec. 2.2. The RPM results in a

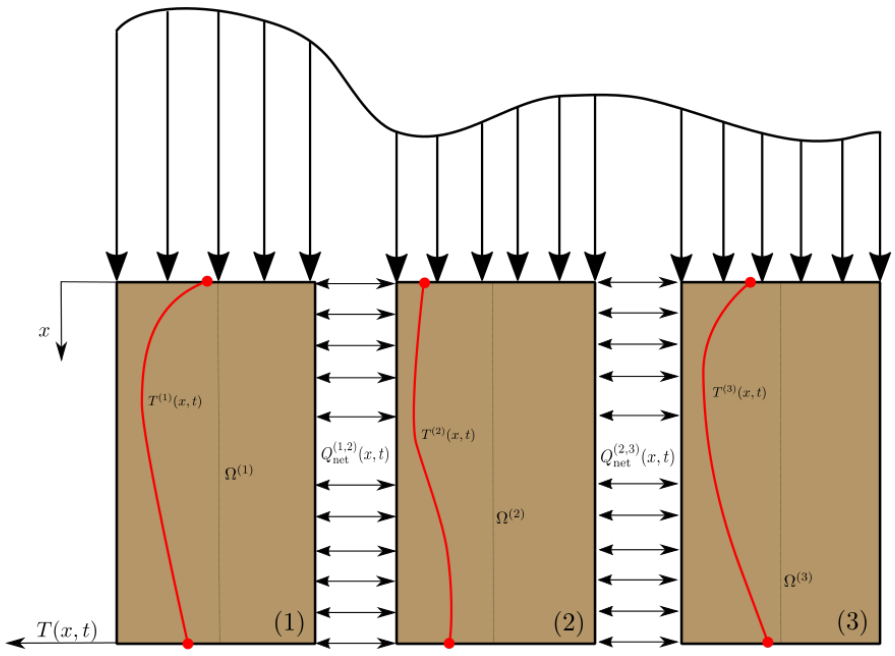

Figure 2: Partition of the TPS into three one-dimensional components.

block-diagonal system of ODEs for the nodal temperature values on the three components, and is given as,

$$\mathbf{A}\left(\mathbf{u}\right)\dot{\mathbf{u}} + \left(\mathbf{B} - \mathbf{C}(t)\right)\mathbf{u} = \mathbf{f}(t) \tag{4}$$

where the block matrices are defined as,

$$\mathbf{A}_{ij} = \begin{cases} \mathbf{A}^i(\mathbf{u}^{(i)}), & i = j \\ 0, & i \neq j \end{cases}, \quad \mathbf{B}_{ij} = \begin{cases} \mathbf{B}^{(i)}(\mathbf{u}^{(i)}), & i = j \\ 0, & i \neq j \end{cases} \tag{5}$$

The details involving the RPM derivation are provided in Appendix.

The ablation on the i-th component is modeled using a one-dimensional approximation to the temperature and mesh-motion equations in eq. (1h), and are given by,

$$\rho c_p \left(\frac{\partial T^{(i)}}{\partial t} - v^{(i)}(x,t) \frac{\partial T^{(i)}}{\partial x} \right) - \frac{\partial}{\partial x}\left(k \frac{\partial T^{(i)}}{\partial x} \right) - \mathcal{Q}^{(i)}_{\text{net}}(x,t) = 0 \tag{6a}$$

$$\frac{\partial}{\partial x}\left(\frac{\partial u^{(i)}}{\partial x} \right) = 0 \tag{6b}$$

with boundary conditions for the energy equation,

$$-k \frac{\partial T^{(i)}}{\partial x}\bigg|_{x=0} = q_b^{(i)}(t) \tag{7a}$$

$$-k \frac{\partial T^{(i)}}{\partial x}\bigg|_{x=\ell} = 0 \tag{7b}$$

and for the elasticity equation,

$$u^{(i)}(0,t) = \int_{t_0}^{t} v^{(i)}(\tau) d\tau = \int_0^t f(T_w^{(i)}(\tau)) d\tau \tag{8a}$$

$$u^{(i)}(\ell,t) = 0 \tag{8b}$$

where $v^{(i)}(t)$ is the surface receding velocity due to ablation, which is a function of the surface temperature as in eq. (2). The surface velocity is computed from a cubic spline interpolate to a B' look-up table...

The coupling between the one-dimensional strands is enforced through the net volumetric energy source term $\mathcal{Q}^{(i)}_{\text{net}}$, which is computed as,

$$\mathcal{Q}^{(i)}_{\text{net}}(x,t) = \sum_j \mathcal{Q}^{(i)}_{\text{in},j}(x,t) - \sum_j \mathcal{Q}^{(i)}_{\text{out},j}(x,t) \tag{9}$$

For example, in the $i = 2$ component of Fig. x, the net volumetric energy source term is,

$$\begin{aligned}\mathcal{Q}^{(2)}_{\text{net}}(x,t) &= \sum_j \mathcal{Q}^{(2)}_{\text{in},j}(x,t) - \sum_j \mathcal{Q}^{(2)}_{\text{out},j}(x,t) \\ &= \mathcal{Q}^{(1,2)}(x,t) - \mathcal{Q}^{(2,3)}(x,t)\end{aligned} \tag{10a}$$

In this work, the volumetric energy source term between the i-th and j-th components is approximated as,

$$\mathcal{Q}^{(i,j)}(x,t) = \frac{T^{(j)}(x,t) - T^{(i)}(x,t)}{R_{ij}} \tag{11}$$

where R_{ij} is the so-called thermal resistance. Empirically, for a component of isotropic heat conductivity k, length L and cross-section A, the thermal resistance is $R = L/kA$. Between components i and j, define $R_{ij} = R_i + R_j$.

Along the one-dimensional domain, a numerical solution based on FEM is adopted for the energy equation, while an analytical solution is adopted for the pseudo-elastic mesh motion. The quasi-steady boundary conditions for the mesh motion are employed via a spline fit to the B' and enthalpy tabulated data as a function of surface temperature. The main results of the numerical approach are presented here and the reader is directed to Sec. A for details.

2.3.1 Thermal Solver

The FEM implementation details are supplied in Appendix x. For the n-th component, the result of the FEM discretization is a system of ODEs for the nodal temperatures, coupled to the neighboring component $n+1$ through the energy volumetric source term,

$$\mathbf{A}^{(i)}\frac{d\mathbf{T}^{(i)}}{dt} + \left(\mathbf{B}^{(i)} - \mathbf{C}^{(i)}(t)\right)\mathbf{T}^{(i)} = \mathbf{f}^{(i)}(t) \tag{12}$$

where,

- $\mathbf{A}^{(i)} \in \mathbb{R}^{M\times M}$ is the mass matrix,
- $\mathbf{B}^{(i)} \in \mathbb{R}^{M\times M}$ is the stiffness matrix,
- $\mathbf{C}^{(i)}(t) \in \mathbb{R}^{M\times M}$ is the advection matrix,,
- $\mathbf{T}^{(i)} \in \mathbb{R}^{M}$ is the vector of nodal temperatures, and
- $\mathbf{f}^{(i)}(t) \in \mathbb{R}^{M}$ is the input vector, which includes the Neumann boundary conditions and the net volumetric energy source term $\mathcal{Q}^{(i)}_{\text{net}}$.

where M is the number of nodes in the one-dimensional mesh for the i-th component.

2.3.2 Pseudo-Elastic Solver

Note that eq. (6b) is steady. Under the assumption that the mesh deformation is quasi-steady, it can be applied at each time step within an ablation simulation. For instance, a known value of the wall temperature $T_w(t)$ specifies a Dirichlet boundary condition for the displacement, and the resulting nodal displacements within the ablator are determined from eq. (1b).

Along the one-dimensional domain, the PDE in eq. (1b) simplifies to,

$$\frac{\partial^2 u^{(e)}}{\partial x^2} = 0 \tag{13}$$

which has the analytical solution,

$$u^{(e)}(x,t) = a(t)x + b(t) \tag{14}$$

Imposing the boundary conditions leads to,

$$u^{(e)}(x,t) = u^{(e)}(0,t)\left(\frac{x_1^{(e)} - x}{h^{(e)}}\right) \tag{15}$$

The mesh velocity is the time derivative of the displacement,

$$v^{(e)}(x,t) = \frac{\partial u^{(e)}(x,t)}{\partial t} = v^{(e)}(t)\left(\frac{x_1^{(e)} - x}{h^{(e)}}\right) \tag{16}$$

2.3.3 Coupling Scheme

2.3.4 Reduced-Physics Ablation Simulation

A Numerical Implementation

A.1 Full-Order Model

A.2 Reduced-Physics Model

This section outlines the DG-FEM implementation for the RPM with $N = 3$ inter-connected one-dimensional components used in Sec. x. Consider the splitting of the TPS as in Fig. x. Over the i-th element with $x \in \Omega^{(i)}(t)$, consider the following linear basis set $\phi_k^{(i)}(x)$ with $k = 1, 2$ on the element $[x_0^{(i)}(t), x_1^{(i)}(t)]$ with length $h^{(i)}(t) = x_1^{(i)}(t) - x_0^{(i)}(t)$. For notational convenience, the time dependence of the spatial domain due to ablating surfaces is dropped. The orthogonal basis functions are defined as,

$$\phi_1^{(i)}(x) = 1, \quad \phi_2^{(i)}(x) = \frac{2}{h^{(i)}}\left(x - x_c^{(i)}\right) \tag{17}$$

where $x_c^{(i)} = (x_0^{(i)} + x_1^{(i)})/2$. Let,

$$x(\xi) = \frac{1-\xi}{2}x_0^{(i)} + \frac{1+\xi}{2}x_1^{(i)}$$

thus for $\xi \in [-1, 1]$,

$$\hat{\phi}_1^{(i)}(\xi) = 1, \quad \hat{\phi}_2^{(i)}(\xi) = \xi \tag{18}$$

Multiply through by the weight function $\phi_j(x)$ and integrate over the domain $\Omega^{(i)}$,

$$\int_\Omega \left[\rho c_p\left(\frac{\partial T^{(i)}}{\partial t} - v^{(i)}(x,t)\frac{\partial T^{(i)}}{\partial x}\right) - \frac{\partial}{\partial x}\left(k\frac{\partial T^{(i)}}{\partial x}\right) - \mathcal{Q}_{\text{net}}^{(i)}(x,t)\right]\phi_l^{(i)}(x)dx = 0 \tag{19}$$

Using integration by parts the natural boundary conditions are obtained,

$$\int_\Omega \rho c_p \left(\frac{\partial T^{(i)}}{\partial t} \phi_l^{(i)}(x) - v(x,t) \frac{\partial T^{(i)}}{\partial x} \phi_l^{(i)}(x) \right) dx + \int_\Omega k \frac{\partial T^{(i)}}{\partial x} \frac{\partial \phi_l^{(i)}(x)}{\partial x} dx = k \frac{\partial T^{(i)}}{\partial x} \phi_l^{(i)}(x) \Big|_{\partial\Omega} + \int_\Omega \phi_l^{(i)}(x) \mathcal{Q}(x,t) dx \tag{20}$$

Perform the finite-element approximation,

$$T^{(i)}(x,t) \approx \sum_{k=1}^{n^{(i)}} u_k^{(i)}(t) \phi_k^{(i)}(x) \tag{21}$$

and define the matrix elements,

$$A_{kl}^{(i)} = \int_\Omega \rho c_p \phi_k^{(i)}(x) \phi_l^{(i)}(x) dx \tag{22}$$

$$B_{kl}^{(i)} = \int_\Omega k \frac{\partial \phi_k^{(i)}(x)}{\partial x} \frac{\partial \phi_l^{(i)}(x)}{\partial x} dx \tag{23}$$

$$C_{kl}^{(i)}(t) = \int_\Omega \rho c_p v^{(i)}(x,t) \phi_k^{(i)}(x) \frac{\partial \phi_l^{(i)}}{\partial x} dx \tag{24}$$

$$f_l^{(i)}(t) = k \frac{\partial T}{\partial x} \phi_l^{(i)}(x) \Big|_{\partial\Omega} + \int_\Omega \phi_l^{(i)}(x) \mathcal{Q}_{\text{net}}^{(i)}(x,t) dx \tag{25}$$

The time-dependent finite-dimensional ODE system for nodal temperatures $\mathbf{T}(t)$, including the ALE-induced advection effect from mesh motion, is given as,

$$\mathbf{A} \frac{d\mathbf{T}}{dt} + (\mathbf{B} - \mathbf{C}(t)) \mathbf{T} = \mathbf{f}(t) \tag{26}$$

On the element (e) the expressions for mass, stiffness, advection, and forcing are given as,

$$M_{mn}^{(i)} = \int_{x_i^{(i)}}^{x_{i+1}^{(i)}} \rho c_p \phi_m^{(i)}(x) \phi_n^{(i)}(x) dx = \rho c_p \frac{h^{(i)}}{6} \begin{pmatrix} 2 & 1 \\ 1 & 2 \end{pmatrix} \tag{27}$$

$$K_{mn}^{(i)} = \int_{x_i^{(i)}}^{x_{i+1}^{(i)}} k^{(i)} \frac{\partial \phi_m^{(i)}}{\partial x} \frac{\partial \phi_n^{(i)}}{\partial x} dx = \frac{k}{h_e} \begin{pmatrix} 1 & -1 \\ -1 & 1 \end{pmatrix} \tag{28}$$

$$C_{mn}^{(i)}(t) = \int_{x_i}^{x_{i+1}} \rho c_p v(x,t) \frac{\partial \phi_n(x)}{\partial x} \phi_m(x) dx \tag{29}$$

$$f_1^{(i)}(t) = (q(t), 0)^T \tag{30}$$

The thermodynamic interaction between the components is modeled via the net volumetric energy source from eq. (9), which for the three-components in Fig. x are described by,

$$\mathcal{Q}_{\text{net}}^{(1)}(x,t) = -\mathcal{Q}^{(1,2)}(x,t) \tag{31a}$$

$$\mathcal{Q}_{\text{net}}^{(2)}(x,t) = \mathcal{Q}^{(1,2)}(x,t) - \mathcal{Q}^{(2,3)}(x,t) \tag{31b}$$

$$\mathcal{Q}_{\text{net}}^{(3)}(x,t) = \mathcal{Q}^{(2,3)}(x,t) \tag{31c}$$